Internal Excitation Mechanisms of Neutral Atoms and Molecules Emitted from Ion Bombarded Organic Thin Films

C. A. Meserole

Department of Chemistry, The Pennsylvania State University, University Park, Pennsylvania 16802

E. Vandeweert

Laboratorium voor Vaste-Stoffysica en Magnetisme, Katholieke Universiteit Leuven, Celestijnenlaan 200 D, B-3001 Leuven, Belgium

Z. Postawa

Smoluchowski Institute of Physics, Jagellonian University, ul. Reymonta 4, PL 30−059 Krakow 16, Poland

N. Winograd*

Department of Chemistry, The Pennsylvania State University, University Park, Pennsylvania 16802

Received: May 14, 2004; In Final Form: July 16, 2004

Resonance enhanced laser photoionization schemes are employed to ionize C_6H_6 molecules and Ag atoms desorbed from Ag{111} by 8 keV Ar^+ ion bombardment. These schemes allow for probing ground state and internally excited species. Time-of-flight mass spectrometry is utilized to detect the postionized atoms and molecules desorbed in a neutral charge state and for determining their kinetic energy distributions from time-of-flight measurements. We find that internally excited species must originate from near the surface/vacuum interface. The species detected in the ground state may originate from deeper in the sample matrix, as well as from the surface.

Introduction

Desorption induced by energetic particle bombardment is an important phenomenon associated with the characterization and modification of molecular surfaces.[1−3] The details of the desorption process are quite complex, and a robust theory explaining the fundamental energy transfer processes leading to the emission of intact molecules is still under development.[4] Computer simulations suggest that, for organic layers on metal surfaces, intact organic molecules are emitted predominately by ejecting metal atoms via a cooperative uplifting mechanism[5] via ballistic collisions. This scheme allows for simultaneous low energy collisions to desorb the molecule without breaking intramolecular bonds. These simulations also show a correlation between the internal energy and the translational energy of the ejecting molecule.[6]

Since collisions between subsurface and surface species lead directly or indirectly to molecular desorption, it is essential to elucidate energy transfer processes that occur as the incident ion energy is transformed into a cascade of moving particles.[7−9] The nature of these collisions involves direct energy transfer between atoms and includes the exchange of internal energy associated with ground and excited states of metal substrate atoms and vibrationally excited states of molecular species.[5]

During the last several years, laser techniques have been developed to monitor the translational energy and internal energy of excited species, providing much more detailed information than previously possible. For metal targets, metastable excited states have been observed with unusually high intensity.[10,11] A number of models have been put forth to explain their behavior.[10,12,13] These models are generally dependent upon the details of the fine structure states of the metal atoms, and may involve resonance energy transfer processes. A particularly interesting case involves the emission of the excited $4d^9 5s^2\ ^2D_{5/2}$ state of silver which lies 3.75 eV above the ground electronic state.[11,14] The population of this state is unusually large and the kinetic energy (KE) of the emitted species is lower than those found for the ground state. A formation mechanism that involves neutralization of an excited Ag ion containing a d hole has been proposed to explain these observations.[12,13,15]

Spectroscopic studies of molecules desorbed from organic monolayers have also emerged in the last several years.[16−20] In our lab, we have focused on benzene (C_6H_6) adsorbed on Ag{111} as a model system. It is a particularly appropriate system since the adsorption of C_6H_6 on Ag is reversible with temperature and C_6H_6 does not form strong bonds with the Ag surface.[17,21] Using multiphoton resonance ionization, it is possible to monitor the ground vibrational level of C_6H_6 as well as vibrationally excited levels (C_6H_6*) by appropriately tuning the wavelength of the ionizing laser.

The main conclusion from these previous experiments is that the desorption mechanism is strongly dependent upon the coverage of C_6H_6 on the Ag surface.[17] In the low coverage regime, cooperative ballistic collisions between the adsorbed molecules and Ag atoms lead to molecular desorption. Internally excited molecules desorb with more average KE than the ground-state molecules, a result supported by molecular dynamics computer simulations.[6] In the multilayer-adsorption regime, excited state molecules eject with less KE than ground-state molecules. This unusual trend could be explained if excited state molecules emitted from the subsurface environment are ef-

* To whom correspondence may be addressed. E-mail: nxw@psu.edu.

10.1021/jp047928o CCC: $27.50
Published on Web 09/11/2004

fectively quenched to the ground state via collisions with nearby molecules.[19] In this scenario, the KE distribution of ground-state molecules would consist of those molecules emitted via a cooperative ballistic mechanism (fast particles) as well as those emitted due to the presence of a molecular collision cascade or perhaps even thermal processes (slower particles). Only the slower particles would contribute to the KE distribution of excited states since those initiated by the ballistic mechanism are lost by quenching.

Because of the presence of metastable spectroscopic states for both ground and excited levels of Ag and C_6H_6, it is possible to follow energy flow for a variety of experimental configurations during the desorption process with unprecedented detail. Since there are indications that the molecular environment of the desorbing species affects the basic emission mechanisms, it is useful to think about experiments where the original molecular location may be more precisely identified. In this work, we present a series of experiments aimed toward proving that internally excited molecules primarily originate near the surface/vacuum interface, whereas ground-state species originate from deeper within the matrix as well as from the surface region.

The experiments begin by acquiring energy and angle resolved distributions of ground and electronically excited-state Ag atoms. The results of these studies are important since they do not support the notion that excited states are formed via neutralization of the d-hole of an excited Ag ion. The influence of a molecular overlayer on the emission of atomic species is studied by probing Ag atoms desorbed as the Ag{111} surface is buried beneath various exposures of C_6H_6. These results clearly show that the intensity of the excited state is preferentially reduced by collisions with overlayer molecules.

To study molecular desorption, a monolayer of C_6H_6 is first physisorbed to the Ag{111} surface. To determine the relation between the origin of excited molecules and their resulting intensity, the C_6H_6 layer is systematically covered by depositing a film of *sec*-butyl alcohol (sBA) molecules on top of a layer of C_6H_6 molecules. The presence of this inert overlayer allows changes in internal energy, translational energy and yield to be examined in detail. Results of these experiments clearly show that the presence of the overlayer preferentially reduces the intensity of excited molecules relative to ground-state molecules. Finally, we show that the intensity of the excited C_6H_6 molecules is restored to nearly their original KE distribution and intensity by depositing a layer of C_6H_6 on top of the sBA layer. Together, these experiments provide convincing evidence that excited molecules are ejected preferentially from the surface/vacuum interface.

Experimental Section

The experiments are conducted in an ultrahigh vacuum chamber (base pressure $= 1 \times 10^{-10}$ Torr) equipped with low energy electron diffraction (LEED) and laser postionization time-of-flight mass spectrometry. Although the details of the apparatus can be found elsewhere,[22] a brief discussion is presented here. The sample is bombarded with 200 ns pulses of Ar^+ ions from a modulated 15 μA continuous ion beam that is accelerated to 8 keV and is focused to a 3 mm spot on the sample surface. The total Ar^+ ion dose is restricted to $\sim 10^{11}$ Ar^+ ions/cm^2 in order to minimize the accumulation of surface damage. The desorbed neutral species are postionized with a laser beam that is focused to a ribbon (1 mm $\times$ 10 mm cross section) parallel to and about 1 cm in front of the sample plane. Laser pulses are produced by frequency doubling the output of a Nd:YAG-pumped tunable dye laser. The laser pulses are characterized by 1 mJ of energy per 6 ns pulse.

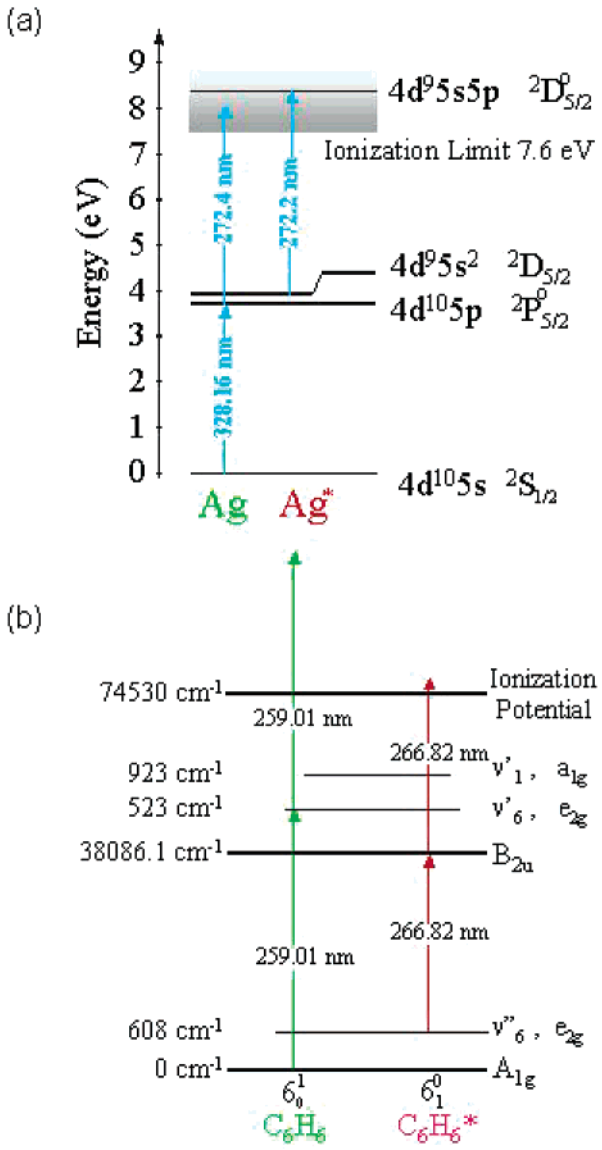

Figure 1. Simplified energy level diagrams and ionization pathways for (a) Ag atoms and (b) C_6H_6 molecules. The scheme for probing Ag atoms in the atomic ground state is indicated by "Ag". The scheme for probing Ag atoms in a highly excited metastable state is indicated by "Ag*". The scheme for probing C_6H_6 molecules in the ground state is indicated by "C_6H_6". The scheme for probing C_6H_6 molecules in a vibrationally excited state is indicated by "C_6H_6*".

Photoionized particles are mass selectively detected on a gated, position sensitive microchannel plate detector. The signal amplitude of the particles emitted to $\pm 20°$ of the surface normal is recorded as a function of the time delay between the Ar^+ ion impact and the laser postionization event in order to generate time-of-flight (TOF) distributions of the neutral molecules. Energy and angle resolved distributions are obtained for the Ag atoms by measuring the mass-selected signal amplitude as a function of position on the MCP and of time delay between the ionization event and ion impact. The ion beam impacts the surface at an incidence angle of 45° for the TOF experiments probing C_6H_6 molecules and 0° for the energy and angle resolved (EARN) experiments probing the Ag atoms.

A simplified energy level diagram of Ag atoms, along with the ionization pathways, is illustrated in Figure 1a. A two-color two-photon and a one-photon one-color ionization scheme are employed for photoionization.[23] The $4d^{10}5s\ ^2S_{1/2}$ ground-state

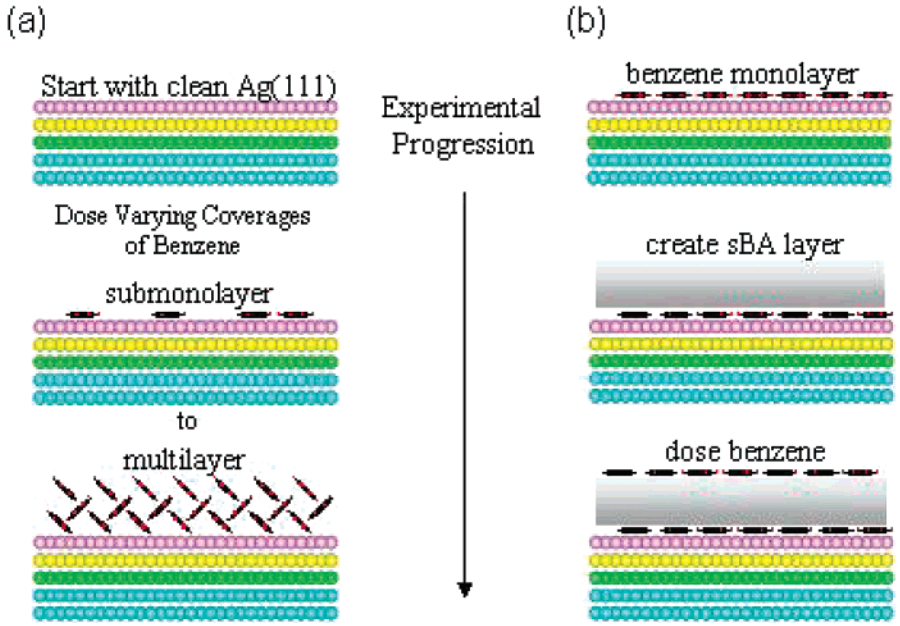

Figure 2. Sample construction schemes for probing (a) Ag atoms and (b) C_6H_6 molecules. The various colors of the substrate atoms allow the layers to be easily distinguished.

atoms (labeled Ag) are first excited into the $4d^{10}5p\ ^2P_{3/2}$ intermediate state by the absorption of a photon having a wavelength of 328.2 nm and subsequently nonresonantly ionized by a second photon having a wavelength of 272.4 nm. Laser pulses from two different lasers are simultaneously overlapped in both time and space in order to accomplish the two-photon two-color photoionization. The metastable atoms (Ag*) in the $4d^95s^2\ ^2D_{5/2}$ state are efficiently ionized by pumping them into the $4d^95s5p\ ^2D_{5/2}$ autoionizing state using only one photon having a wavelength of 272.2 nm. Photoionization is not saturated for either Ag or Ag*, so it is not possible to compare absolute intensities of these two species.

Ionization schemes for probing C_6H_6 molecules are depicted in a simplified energy level diagram of C_6H_6 illustrated in Figure 1b. Neutral C_6H_6 molecules desorbed in the first vibrationally excited state of the ν_6'' mode, lying ~0.1 eV above the molecular ground state,[24] are ionized with 266.8 nm radiation. Benzene molecules desorbed in the molecular ground state are probed with 259.0 nm radiation.

The Ag single crystal is sputter cleaned with a defocused Ar^+ ion beam for several cycles (~15 μA, 8 keV, 5 min/cycle) and annealed at 730 K prior to the experiments. The C_6H_6 and sBA samples are treated by several freeze−pump−thaw cycles in order to remove gaseous impurities prior to dosing into the chamber. Two separate dosing manifolds equipped with separate leak valves are used to avoid the possibility of vapor contamination in the source manifolds. The vapors are dosed by a controlled leak into the vacuum chamber to a specific pressure (which is uncorrected for the ion gauge sensitivity) for a specific time period after the Ag crystal has been cooled to about 120 K. The vapor doses or exposures are reported in langmuir units (1 langmuir = 1×10^{-6} Torr·s).

Several factors have been considered in the selection of sBA for these experiments. Since sBA (74.12 g/mol) has a lower molecular mass than C_6H_6 (78.11 g/mol), no isobaric interferences with C_6H_6 can result if sBA undergoes photofragmentation. The similar masses of the sBA and C_6H_6 are important for momentum transfer issues. The capacity of internal energy storage should be comparable for C_6H_6 and sBA, since they have a similar number of vibrational modes ($n_{C_6H_6} = 30$ and $n_{sBA} = 39$). Because the vapor pressure of sBA is lower than that of C_6H_6,[25] which forms a stable target system in a vacuum, sBA will also form a stable target system and not rapidly vaporize. It has been reported that *n*-butanol reversibly physisorbs to Ag{110}, and the alcohol molecules in a monolayer lie parallel to the Ag{110} surface.[26] Therefore, the sBA molecules should not form strong bonds with the Ag{111} surface via chemisorption, especially not via a dissociative chemisorption pathway that would significantly alter the simplicity of the chemical system. Additionally, the sBA molecules are fairly transparent in the UV region employed to ionize C_6H_6. The ionization potential of sBA is near 10 eV,[27] and nonresonant ionization of sBA by the wavelengths employed for the ionization of C_6H_6 would require a three-photon process. This event is very unlikely because the magnitude of the cross section for a three-photon ionization process is approximately 10^{-80} cm^6 s^2, compared to 10^{-50} cm^4 s for a two-photon process.[28]

The general progression of sample construction for probing Ag atoms and C_6H_6 molecules is illustrated in Figure 2, parts a and b, respectively. A clean Ag substrate cooled to about 120 K is utilized in the first phase of the experiments. After mass, energy, and angle distributions are obtained from a clean Ag sample, C_6H_6 is dosed on the Ag surface. The amount dosed is varied during the course of the complete set of experiments. Then, relevant spectra of the atoms are obtained again. Probing C_6H_6 molecules in various chemical environments requires a more elaborate scheme. After the Ag crystal is exposed to a 7 langmuir dose of C_6H_6, mass spectra and quantum state resolved C_6H_6 TOF distributions are obtained for reference. Next, the sample is dosed with sBA, and mass spectra and C_6H_6 TOF distributions are obtained again. Finally, an additional 7 langmuir exposure of C_6H_6 is dosed onto this construct, and identical measurements are performed.

Results and Discussion

The EARN distributions of Ag atoms emitted in the ground state and in the excited state are shown in Figure 3, parts a and c, respectively. The intensity of the Ag atoms peaks in the off-normal direction due to channeling and blocking by other first

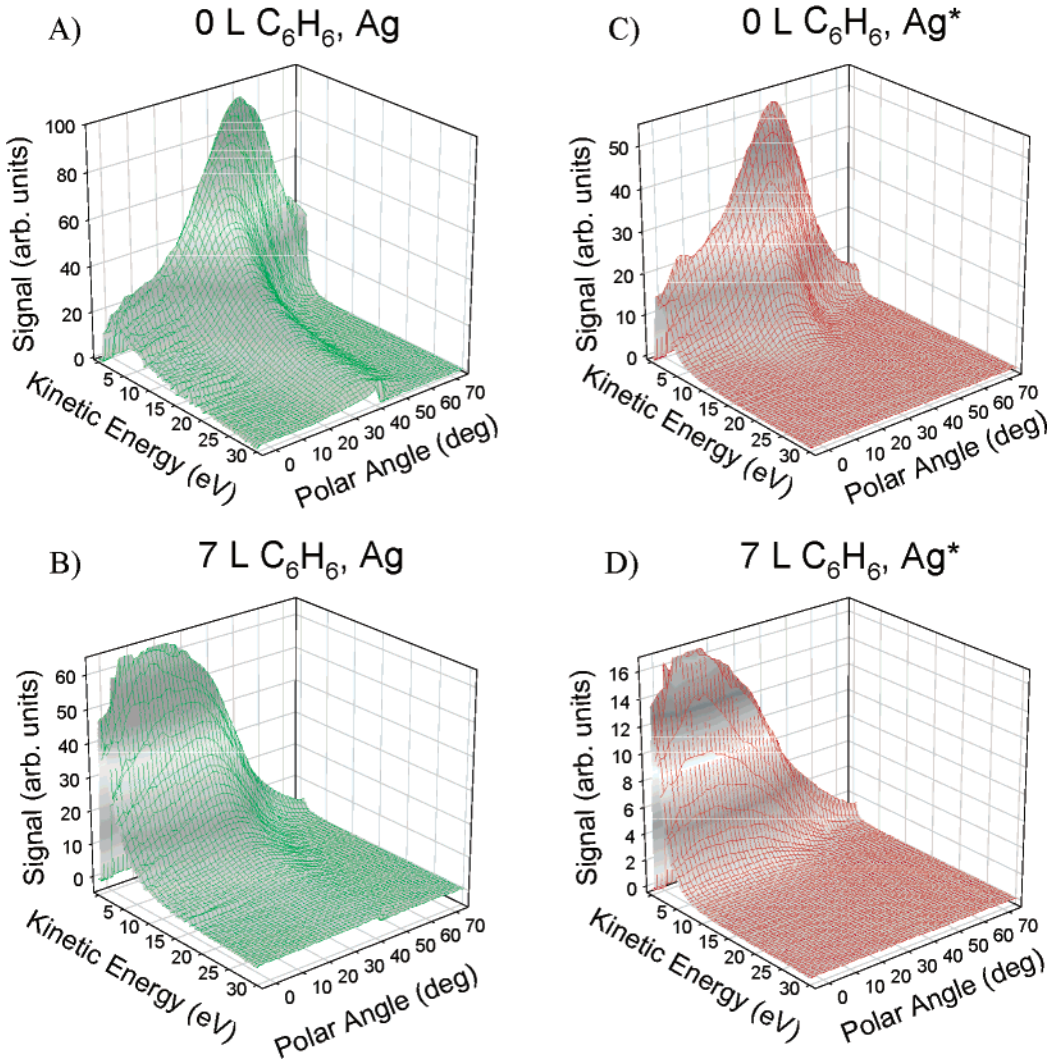

Figure 3. Energy and angle resolved distributions of Ag atoms. Distributions for the ground-state atoms are represented in panels a and b. Distributions for the metastable atoms are represented in panels c and d. Distributions from a clean, cold Ag(111) surface are in panels a and c. Distributions from an Ag(111) surface exposed to 7 langmuir of C_6H_6 are in panels b and d.

layer atoms. This effect will be discussed in more detail later in this section. In general, these results support those of Berthold and Wucher[14,23,29] who showed that the KE distribution of Ag* exhibits a narrower distribution than that of Ag. Preliminary measurements suggested a weak dependence of the ratio of the Ag* intensity to the Ag intensity on emission angle. These workers also showed that approximately 6% of the total flux of sputtered atoms is populated by Ag* ejected in the metastable $4d^95s^2\ ^2D_{5/2}$ state with an excitation energy of 3.75 eV above the ground state. The results were partly explained as arising from the resonant neutralization of sputtered secondary ions containing a d-hole. Although this model is consistent with the observed KE distributions, it is in disagreement with the polar angle dependence. Subsequent models have suggested that Ag* is formed directly by collisions in the solid.[12,13] Computer simulations for this scheme show a narrowing of the KE distribution of Ag*, anomalously high intensities, and a weak dependence on polar angle.[13]

The population of the excited state relative to the ground state, P*, is defined as the Ag* ($=4d^95s^2\ ^2D_{5/2}$) signal divided by the Ag signal. The dependence of P* on the KE and on the polar angle of the ejecting Ag atoms is depicted in Figures 4 and 5, respectively. In accordance with the neutralization model described previously, P* decreases as a function of KE and

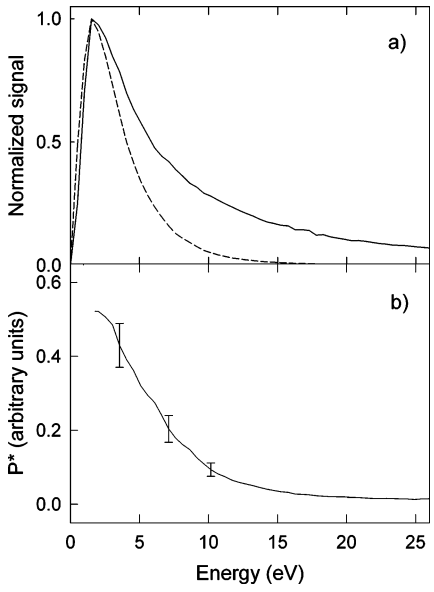

Figure 4. Angle-integrated KE distributions for Ar^+ bombarded clean Ag(111) of (a) metastable state (dotted line) and ground-state Ag atoms (solid line) and (b) the excitation probability, as defined in the text.

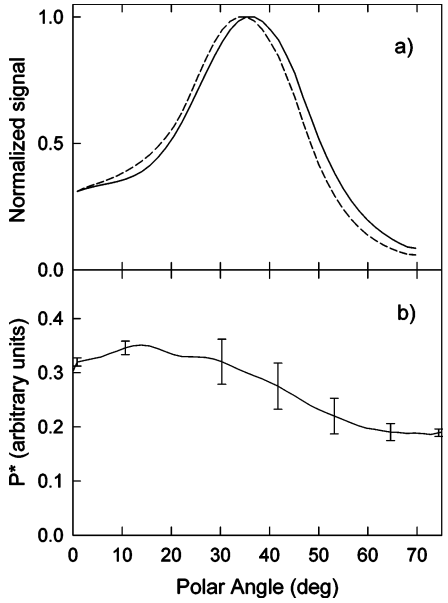

Figure 5. Energy-integrated polar angle distributions for Ar^+ bombarded clean Ag(111) of (a) metastable state (dotted line) and ground-state Ag atoms (solid line) and (b) the excitation probability, as defined in the text.

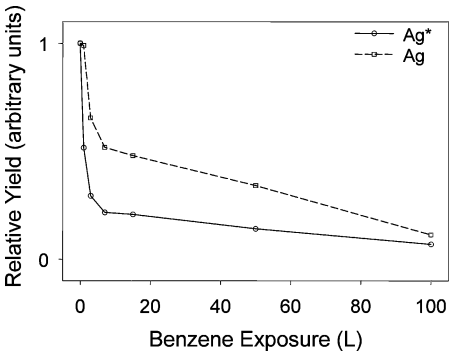

Figure 6. Relative yield of Ag atoms desorbed in the ground state and in the metastable state as a function of C_6H_6 exposure.

exhibits a weak dependence on polar angle. Although a detailed interpretation of these data is beyond the scope of this work, the results certainly support the most recent descriptions of the excited state formation mechanisms.[12,13,15]

The next phase of these experiments is to expose the clean Ag{111} surface to varying amounts of C_6H_6 and to monitor the changes in the internal state distribution of both Ag and C_6H_6. As noted earlier, the EARN distributions for Ag and Ag* desorbed from a clean crystal prior to dosing C_6H_6 are shown in Figure 3, parts a and c, respectively. The resulting EARN distributions for Ag and Ag* after a 7 langmuir exposure of C_6H_6 are shown in Figure 3, parts b and d, respectively. Both the Ag and Ag* polar angle distributions from a clean single crystal show a preferential ejection at a polar angle of about 35°. As the coverage of the C_6H_6 increases, the distribution broadens and shifts toward normal emission angles. However, the shifting and broadening is more pronounced for Ag*.

A decrease in yield is observed for all ejected Ag species as C_6H_6 molecules are dosed onto the surface as illustrated in Figure 6. Note that the yield of Ag* is reduced more rapidly than Ag, presumably because collisional quenching is among the possible deexcitation mechanisms for these atoms. The possibility of collisional quenching implies that a portion of the detected ground-state atoms leave the surface in the metastable state but relax prior to detection. Therefore, the

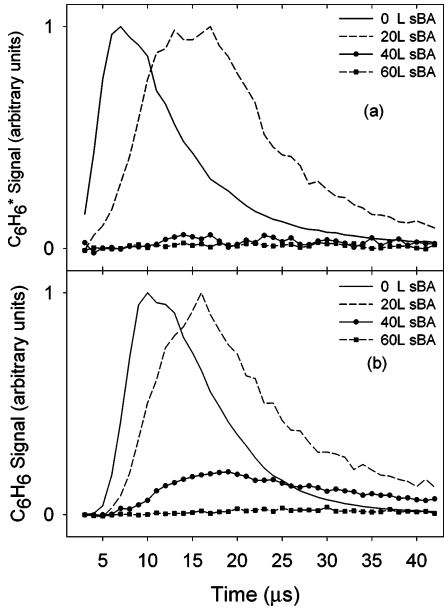

Figure 7. Time-of-flight distributions for sputtered C_6H_6 molecules buried beneath varying exposures of sBA. The top panel (a) represents distributions of molecules detected in a vibrationally excited state. Panel b represents distributions of molecules detected in molecular ground state.

possibility of quenching implies that both the KE and the polar angle distribution of ground-state atoms contain a contribution from Ag* atoms that have been deexcited to ground-state Ag atoms.

The preferential ejection of Ag atoms in the off-normal direction as observed in the polar angle distributions is explained via channeling and blocking of the departing atoms by other first-layer atoms.[30] Since the Ag* distribution is largely depleted of atoms ejected off-normally, it can be argued that these atoms did not survive a collision with a C_6H_6 molecule upon departure. Particles traveling in an off-normal direction will have a higher probability of encountering and colliding with a C_6H_6 molecule than particles that are emitted in a direction normal to the surface. At higher exposures the shift of both Ag and Ag* distributions to a pronounced ejection in the normal direction is indicative that enough collisions with adsorbate molecules occur to randomize the trajectories of the ejected particles.

An additional aspect to consider to explain the distinct features of the Ag* desorption characteristics is the size of Ag* vs the size of Ag. In general, an atom (electron cloud) expands as its energy increases.[31] The Ag* is larger than Ag due to the promotion of an electron into a more distant orbital, resulting in a larger collision cross section. As a result, Ag* will more likely be blocked by C_6H_6 molecules than Ag would be. A larger cross section coupled with the potential for collisional deexcitation suggests that the total yield of Ag* will diminish more rapidly than the Ag yield as a function of C_6H_6 exposure, which is clearly illustrated in Figure 6a.

Deposition of an organic overlayer on top of the C_6H_6 film causes a suppression of the yield of ejected C_6H_6 molecules and reduces their internal energy. Time-of-flight distributions of neutral C_6H_6 molecules desorbed in a vibrationally excited state (C_6H_6*) and in the molecular ground state (C_6H_6) are shown in Figure 7, parts a and b, respectively. In both cases, traces labeled 0 langmuir sBA are the peak normalized reference distributions of C_6H_6 sputtered from a sample prepared by a 7 langmuir exposure to Ag(111). Traces for the 0 and 20 langmuir sBA exposures are peak normalized for easy comparison. The

40 langmuir sBA and 60 langmuir sBA plots are rescaled relative to the 20 langmuir sBA so that relative intensities can be compared. The peak intensity for the 20 langmuir sBA case is reduced by a factor of 5, relative to the 0 langmuir situation. For both C_6H_6* and C_6H_6, the TOF distributions shift toward higher times and broaden as the overlayer becomes thicker. The shifting and broadening indicate the KE distributions of the desorbed C_6H_6 species shift toward lower KE values. Such behavior is expected since C_6H_6 must collide with overlayer molecules for ejection to occur. In addition to changes in the distribution shape, significant changes to the yields of the C_6H_6 species are illustrated in Figure 7. It is especially interesting to note that ejection of excited state molecules is effectively quenched by the sBA overlayer, while a small ground-state C_6H_6 signal is still observable even after 40 langmuir of sBA exposure. Hence, it is clear that C_6H_6 molecules are undergoing direct collisions with sBA overlayer molecules which reduce the probability of C_6H_6 emission, reduce the translational energy through direct energy transfer processes during collisions, and selectively reduce the probability of vibrational excitation through collisional quenching.

Another factor contributing to the reduced C_6H_6 yield is the reduced probability of collisions between C_6H_6 molecules and Ag atoms. As the sBA layer becomes thicker, it more efficiently absorbs energy associated with the incident Ar^+ ions, reducing the excitation of substrate Ag atoms. In the energy ranges involved with these studies, there is a general trend that the sputter yield increases with increasing primary ion energy.[32] Fewer dislocated silver species will necessarily generate a smaller number of collisions with C_6H_6 molecules that lead to the energetic emission of C_6H_6. As a result, the energy distribution of the C_6H_6 molecules is depleted of higher KE molecules (i.e., the KE distribution will shift toward lower values).

The sBA molecules serve a dual role in the overall process of the emission of C_6H_6 molecules buried beneath the sBA matrix. By way of reducing the Ar^+ ion energy before it reaches the C_6H_6/Ag interface, the sBA molecules reduce the number of C_6H_6 molecules initially set into motion via ballistic collisions with substrate species. Then a portion of the C_6H_6 molecules set into motion by ballistic collisions near the Ag surface are blocked by the sBA overlayer.

A C_6H_6 overlayer on Ag(111) affects the emission of the desorbed Ag monomers in much the same way sBA affects desorbed C_6H_6 molecules. There is a strong similarity to the trends observed for the C_6H_6 molecules and the trends of Ag monomers desorbed in the atomic ground state (Ag, $4d^{10}5s\ ^2S_{1/2}$) and in a highly excited metastable state (Ag*, $4d^95s^2\ ^2D_{5/2}$) as the Ag surface is buried deeper under increasingly thicker cap of C_6H_6 molecules. The TOF distributions of Ag and of Ag* for a variety of C_6H_6 exposures are shown in Figure 8, parts c and d. The TOF distributions of C_6H_6 and of C_6H_6* buried beneath a variety of sBA exposures are shown in Figure 8, parts a and b for comparison to Ag and Ag*. The TOF distributions of both Ag and Ag* shift toward higher times and broaden as the C_6H_6 exposure is increased. Also, the Ag and Ag* yields decrease with increasing C_6H_6 exposure. Another similarity between the C_6H_6 and the Ag distributions is that in both cases the influence of the overlayer appears to affect the emission of the excited species more than the ground-state species. Collisions between the Ag atoms and the molecules of the C_6H_6 layer reduce the atom yields and deplete the atoms of KE. Collisional deexcitation, as well as size effects, lead to a more efficient yield reduction of Ag*.

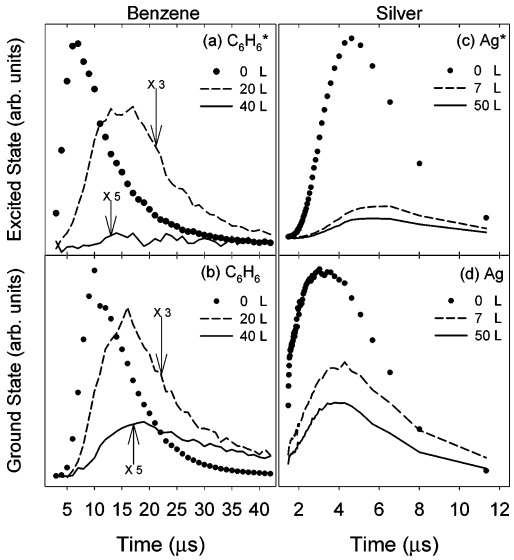

Figure 8. Time-of-flight distributions of C_6H_6 molecules and Ag atoms buried beneath various exposures of organic molecules. The C_6H_6 molecules (a, b) are buried beneath sBA molecules. The Ag atoms (c, d) are buried beneath C_6H_6 molecules. Distributions of species detected in an excited state are represented in the top panels (a and c). Distributions of species detected in the ground state are represented in the bottom panels (b and d).

Another part of the puzzle of molecular emission is how molecules are desorbed from the surface of a thick organic (or molecular) system. In prior experiments, the system progressively becomes more organic in nature by increasing the C_6H_6 exposure.[17,33] Several mechanisms responsible for desorbing slow molecules from the thicker C_6H_6 layers are proposed. Collisions between the molecules and the primary ion, mobile fragments, and/or dislocated Ag atoms are suspected of developing a molecular collision cascade leading to the emission of slow molecules from the surface.[8] A thermal mechanism as a result of exothermic reactions has also been suggested.[16] All these mechanisms generate the emission of slow molecules.

To prove that analyte molecules, especially those that are internally excited, are desorbed from the very top layer of a thick organic surface where ballistic collisions between substrate atoms and analyte molecules are largely absent (especially in the very thick exposures of sBA), an additional 7 langmuir exposure of C_6H_6 is administered to the sBA layers. The TOF distributions for C_6H_6* and C_6H_6 desorbed from the surface of a variety of sBA exposures are shown in Figure 9, parts a and b, respectively. Again, similar trends are observed in both cases. As the exposure is increased, the TOF distributions shift toward higher times, and the yields decline as the sBA exposure is increased. For exposures around 30 or 40 langmuir of sBA, C_6H_6 and C_6H_6* yields decline appreciably from those obtained from a 20 langmuir sBA exposure. The TOF distributions, especially those from the C_6H_6*, are significantly depleted of high KE particles (i.e., particles with flight times below $\sim$12 μs). This result is not unexpected since it is in this exposure regime that the yield of Ag substrate species is approximately the same as the substrate yields when the organic matrix is comprised of a 150 langmuir exposure of pure C_6H_6 (Figure 6b). This relation suggests that sBA is more opaque than C_6H_6 on a per Langmuir basis. In the case of a 150 langmuir exposure of pure C_6H_6, a slight shift in the C_6H_6 KE distribution is observed, whereas a dramatic change in the C_6H_6* energy distribution is seen. A similar observation is seen in the 30−40 langmuir sBA exposure.

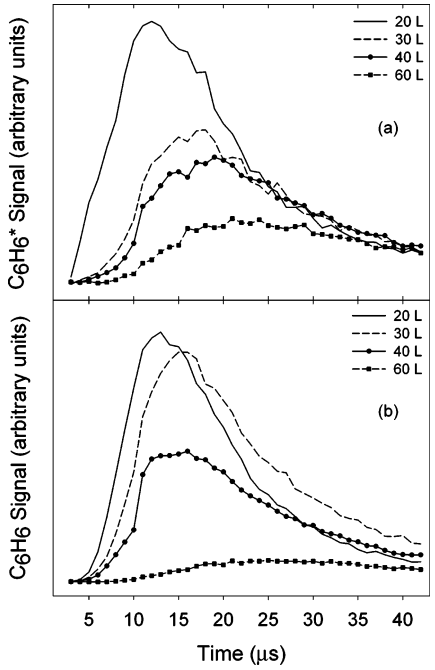

Figure 9. Time-of-flight distributions of C_6H_6 molecules desorbed from a layer of sBA molecules. Distributions of C_6H_6 molecules desorbed in a vibrationally excited state are represented in panel a. Distributions of benzene molecules desorbed in the molecular ground state are represented in panel b. The C_6H_6 layer is created by dosing a 7 langmuir exposure of C_6H_6 molecules on top of the sBA layers created by varying exposures of the sBA molecules.

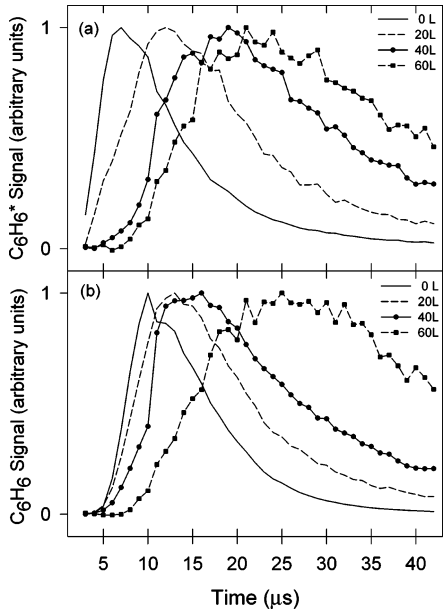

Figure 10. Peak normalized TOF distributions of C_6H_6 molecules desorbed from a layer of sBA molecules. Distributions of C_6H_6 molecules desorbed in a vibrationally excited state are represented in panel a. Distributions of C_6H_6 molecules desorbed in the molecular ground state are represented in panel b. The C_6H_6 layer is created by dosing a 7 langmuir exposure of C_6H_6 molecules on top of the sBA layers created by varying exposures of the sBA molecules. These plots exemplify how the time distributions shift as the molecular overlayer becomes thick due to increased exposure of molecules.

The peak normalized TOF distributions of C_6H_6* and C_6H_6 from a system where the C_6H_6 molecules are near the vacuum interface are shown in Figure 10. The peak normalized distributions better illustrate the dramatic shift and broadening as the sBA exposure is increased. The TOF distributions of C_6H_6 molecules desorbed from a system comprised of only a 7 langmuir C_6H_6 exposure on Ag(111) (marked as 0 langmuir of exposure with sBA) are shown for the sake of comparison. It is evident that the C_6H_6* emission is extremely sensitive to the nature of the system. As the sBA gets thicker, the high KE C_6H_6* emissions from the C_6H_6/Ag interface are quenched rapidly. (This is seen by the decay of the TOF distribution amplitude in the low time, ≤ 10 μs, portion of the plot.) As the ballistic component of the C_6H_6* emission is quenched, only slow molecules from the surface/vacuum interface can account for the C_6H_6* signal. On the other hand, C_6H_6 emissions are less affected by the presence of the sBA overlayer and the ballistic component resulting from collisions between substrate atoms and C_6H_6 molecules is still visible in the ground-state emissions for sBA exposures up to 40 langmuir. The TOF distributions for C_6H_6 and C_6H_6* are virtually identical after 60 langmuir sBA exposure. This result clearly demonstrates that a common, low KE mechanism, such as localized heating or a molecular collision cascade, is responsible for the desorption of both C_6H_6 and C_6H_6* from very thick organic samples. This new mechanism does not involve contributions from ballistic processes taking place near the organic/Ag interface. It should be noted that, in the case of a pure C_6H_6 matrix, the exposure of C_6H_6 would need to be significantly greater than 150 langmuir for this situation to arise.

Conclusions

In this work, we have probed the internal energy distribution of atoms and molecules desorbed from ion bombarded surfaces. The results show that it is possible to acquire high quality data for excited states of Ag atoms and for vibrationally excited C_6H_6 molecules. For the case of Ag, the excited atoms exhibit a narrower KE distribution than the ground-state atoms, anomalously high intensities, and the excitation probability exhibits a weak dependence of yield on polar angle of ejection. The results are shown to be consistent with recent models that suggest that Ag* is formed directly by collisions in the solid, rather than by a resonant electron tunneling model.

With respect to molecular desorption, we concentrate on the behavior of molecular overlayers covered with an inert molecular buffer layer to monitor the relevant energy transfer processes. We find that this buffer layer acts as an energy sink with respect to species that are desorbed from a location between the buffer layer and the bulk of the sample. Collisions between the desorbing species and the buffer species result in molecules or atoms with lower average KE and lower internal energy being propagated into the vacuum. Moreover, these collisions tend to suppress the yield of the species buried beneath the buffer layer. Additionally, emission of species that do make it into the vacuum is observed preferentially in the normal direction. This distribution is observed even if the species of interest originates in a single crystal, which typically has pronounced off-normal emissions.

The presence of the buffer layer acts to suppress the yield of internally excited species. Only the molecules located near the surface/vacuum interface have a good chance of entering into the vacuum in an internally excited state. This is not the case for molecules or atoms in the ground state, however. These can initially be located deeper in the bulk of the sample. Of course, some portion of the species detected in the ground state may have started out in an excited state but were relaxed into the ground state after collisions with the buffer layer molecules.

This regional or spatial sensitivity could become the basis for learning something about the location of an analyte molecule

when it is in the surface region. Our study shows that there is a direct link between the original location of the analyte and KE distribution, as well the internal energy distribution. The distinct aspect of this observation is that the depth information could be acquired while still in the static sputtering regime, and without disrupting the surface structure. In addition, our data show that by examining the internally excited species, sensitivity is gained toward analyzing only the species residing near the surface/vacuum interface. Thus, laser probing based on resonant ionization schemes such as the ones developed here could become a tool for *surface*, not just near surface, analysis.

Finally, we have demonstrated that the application of a physisorbed mask material may be utilized to dictate the population partitions of the internal energy distribution of the desorbed species. Both sBA and C_6H_6 molecules were used as masking agents. Both species were effective at significantly reducing the population of the detectable excited state species. This may prove beneficial in experiments where the emission of internally cool, and thus extremely stable, molecules must be generated.

Acknowledgment. The financial support from the National Institutes of Health and the National Science Foundation, and the Polish Committee for Scientific Research (Fund no. 3T09A12426), ACK CYFRONET and Cooperation Program between Flanders and Poland are gratefully acknowledged. E.V. is a postdoctoral fellow of the Fund for Scientific Research-Flanders (Belgium). The authors would also like to thank B. J. Garrison for helpful discussions.

References and Notes

(1) Benninghoven, A. *Surf. Sci.* **1994**, *300* (1−3), 246−260.
(2) Ruschenschmidt, K.; Schnieders, A.; Benninghoven, A.; Arlinghaus, H. F. *Surf. Sci.* **2003**, *526* (3), 351−355.
(3) Grade, H.; Winograd, N.; Cooks, R. G. *J. Am. Chem. Soc.* **1977**, *99*, 7725−7726.
(4) Delcorte, A.; Vanden Eynde, X.; Bertrand, P.; Vickerman, J. C.; Garrison, B. J. *J. Phys. Chem. B* **2000**, *104*, 2673−2691.
(5) Garrison, B. J.; Delcorte, A.; Krantzman, K. D. *Acc. Chem. Res.* **2000**, *33*, 69−77.
(6) Chatterjee, R.; Postawa, Z.; Winograd, N.; Garrison, B. J. *J. Phys. Chem. B* **1999**, *103*, 151−163.
(7) Urbassek, H. M. *Nucl. Instrum. Methods Phys. Res., Sect. B* **1997**, *122*, 427−441.
(8) Krantzman, K. D.; Postawa, Z.; Garrison, B. J.; Winograd, N.; Stuart, S. J.; Harrison, J. A. *Nucl. Instrum. Methods Phys. Res., Sect. B* **2001**, *180*, 159−163.
(9) Harrison, D. E. *CRC Crit. Rev. Solid State Mater. Sci.* **1988**, *14*, S1−S78.
(10) Wucher, A.; Sroubek, Z. *Phys. Rev. B* **1997**, *55* (2), 780−786.
(11) Garrison, B. J.; Winograd, N.; Chatterjee, R.; Postawa, Z.; Wucher, A.; Vandeweert, E.; Lievens, P.; Philipsen, V.; Silverans, R. E. *Rapid Commun. Mass Spectrom.* **1998**, *12* (18), 1266−1272.
(12) Staudt, C.; Wucher, A.; Bastiaansen, J.; Philipsen, V.; Vandeweert, E.; Lievens, P.; Silverans, R. E.; Sroubek, Z. *Phys. Rev. B* **2002**, *66* (8), art. no.-085415.
(13) Wojciechowski, I.; Garrison, B. J. *Surf. Sci.* **2003**, *527* (1−3), 209−218.
(14) Berthold, W.; Wucher, A. *Phys. Rev. Lett.* **1996**, *76*, 2181−2184.
(15) Sroubek, Z.; Sroubek, F.; Wucher, A.; Yarmoff, J. A. *Phys. Rev. B* **2003**, *68* , 115426/1−115426/5.
(16) Chatterjee, R.; Riederer, D. E.; Postawa, Z.; Winograd, N. *Rapid Commun. Mass Spectrom.* **1998**, *12*, 1226−1231.
(17) Chatterjee, R.; Riederer, D. E.; Postawa, Z.; Winograd, N. *J. Phys. Chem. B* **1998**, *102*, 4176−4182.
(18) Meserole, C. A.; Vandeweert, E.; Chatterjee, R.; Winograd, N.; Postawa, Z. *Appl. Surf. Sci.* **1999**, *141* (3−4), 339−344.
(19) Meserole, C. A.; Vandeweert, E.; Postawa, Z.; Haynie, B. C.; Winograd, N. *J. Phys. Chem. B* **2002**, *106*, 12929−12937.
(20) Meserole, C. A.; Vandeweert, E.; Postawa, Z.; Dou, Y.; Garrison, B. J.; Winograd, N. *Nucl. Instrum. Methods Phys. Res., Sect. B* **2001**, *180*, 53−57.
(21) Dudde, R.; Frank, K. H.; Koch, E. E. *Surf. Sci.* **1990**, *225* (3), 267−272.
(22) Kobrin, P. H.; Schick, G. A.; Baxter, J. P.; Winograd, N. *Rev. Sci. Instrum.* **1986**, *57*, 1354−62.
(23) Berthold, W.; Wucher, A. *Nucl. Instrum. Methods Phys. Res., Sect. B* **1996**, *115* (1−4), 411−414.
(24) Callomon, J. H.; Dunn, T. M.; Mills, I. M. *Philosophical Transactions of the Royal Society of London, Series A: Mathematical, Physical and Engineering Sciences* **1966**, *259* (1104), 499−532.
(25) Weast, R. C., Ed. *Handbook of Chemistry and Physics*, 54th ed.; CRC: Boca Raton, FL, 1974; p 2436.
(26) Zhang, R.; Gellman, A. J. *J. Phys. Chem.* **1991**, *95*, 7433−7437.
(27) The average value of the ionization potential obtained from the data reported from NIST and found at http://webbook.nist.gov/chemistry.
(28) Morellec, J.; Normand, D.; Petite, G. *Adv. At. Mol. Phys.* **1982**, *18*, 97−164.
(29) Berthold, W.; Wucher, A. *Phys. Rev. B* **1997**, *56*, 4251−4260.
(30) Bernardo, D. N.; Elmaazawi, M.; Maboudian, R.; Postawa, Z.; Winograd, N.; Garrison, B. J. *J. Chem. Phys.* **1994**, *100*, 8557.
(31) Atkins, P. W. *Physical Chemistry*, 4th ed.; W. H. Freeman: New York, 1990.
(32) Behrisch, R.; Wittmaack, K. *Top. Appl. Phys.* **1991**, *64*, 1−13.
(33) Vandeweert, E.; Meserole, C. A.; Sostarecz, A.; Dou, Y.; Winograd, N.; Postawa, Z. *Nucl. Instrum. Methods Phys. Res., Sect. B* **2000**, *164*, 820−826.